

Multi-frequency Phase Unwrapping for Time-of-Flight Cameras

David Droschel, Dirk Holz, and Sven Behnke

Abstract—Time-of-Flight (ToF) cameras gain depth information by emitting amplitude-modulated near-infrared light and measuring the phase shift between the emitted and the reflected signal. The phase shift is proportional to the object's distance modulo the wavelength of the modulation frequency. This results in a distance ambiguity. Distances larger than the wavelength are *wrapped* into the sensor's non-ambiguity range and cause spurious distance measurements.

We apply *Phase Unwrapping* to reconstruct these wrapped measurements. Our approach is based on a probabilistic graphical model. We use loopy belief propagation to detect and infer the position of wrapped measurements. Besides depth discontinuities, our method utilizes multiple modulation frequencies to identify wrapped measurements. In experiments, we show that wrapped measurements are identified and corrected, even in situations where the scene shows steep slopes in the depth measurements.

I. INTRODUCTION AND RELATED WORK

Time-of-Flight (ToF) cameras attracted attention in the field of robotics and automation in the last decade. They are compact, solid-state sensors, which provide depth and reflectance images at high frame rates.

One of the first applications in robotics considering ToF cameras as an alternative to laser scanning has been presented in 2004 by Weingarten *et al.* who evaluated the utility of ToF cameras in terms of basic obstacle avoidance and local path-planning [1]. In 2005, Sheh *et al.* used a ToF camera for human-assisted 3D mapping in the context of the RoboCup Rescue league [2]. Ohno *et al.* used a ToF camera for estimating a robot's trajectory and reconstructing the surface of the environment in 2006 [3]. Recently, May *et al.* presented and evaluated different approaches for registering multiple range images of ToF cameras for fully autonomous 3D mapping [4].

All the aforementioned approaches have shown that the complex error model of ToF cameras requires special attention. The different systematic and non-systematic errors cause, amongst other effects:

- **Measurement noise:** Data from the ToF camera is subject to noise, especially at larger distances and on poorly reflecting objects.
- **Jump edges:** ToF cameras measure a smooth transition, where the transition between one shape to the other is disconnected due to occlusions [4].
- **Distance ambiguity:** ToF cameras employ an array of light emitting diodes (LEDs) that illuminate the environment with modulated near-infrared light. The reflected light is received by a CCD/CMOS chip for every pixel



Fig. 1. Unwrapping the input depth image (left). The brightness encodes the measured distance (dark pixels are near, bright pixels far away). The abrupt change from bright to dark in the input image is the phase jump that we want to detect in order to correct the measured distances and to obtain the unwrapped depth image (right).

in parallel. Depth information is gained by measuring the phase shift between the emitted and the reflected light, which is proportional to the object's distance modulo the wavelength of the modulation frequency. This results in an ambiguity in distance measurements. Measurements larger than the used wavelength are *wrapped* into the sensor's non-ambiguity range and cause artifacts and spurious distance measurements.

As shown by Fuchs and Hirzinger, extrinsic and depth calibration can considerably improve the signal-to-noise ratio of ToF cameras [5]. For detecting jump edges, sufficient results can be achieved by examining, for every measurement, the opposing angles of the triangle spanned by the camera's focal point, the point itself and its local pixel neighborhood [4]. Distance ambiguities, however, have (to the best of our knowledge) not yet been addressed for ToF cameras.

Especially when mapping larger environments where measured distances exceed the wavelength of the modulation frequency, obtaining an unwrapped depth image becomes crucial [4]. Inferring a correct, unwrapped signal from a wrapped signal is also known as *Phase Unwrapping*. That is, depth measurements being erroneously projected into the non-ambiguity range of the sensor are identified and projected back into the correct interval. Phase unwrapping is a fundamental problem in image processing [6] and has been successfully applied in magnetic resonance imaging [7] and interferometric synthetic aperture radar (SAR) [8].

The goal of phase unwrapping is to infer a number of relative *phase jumps* (or phase shifts) from the wrapped signal. A phase jump is defined between two adjacent pixels in x -

and y -direction of the image. Since the unrestricted phase unwrapping problem is ill-posed, most algorithms make *a priori* assumptions to reduce the number of admissible phase jumps. One common assumption is that neighboring measurements are more likely closer to each other than farther apart. With this assumption, phase jumps bringing unwrapped measurements as close together as possible are chosen. However, even in the absence of noise, situations may arise where a decision cannot be made that is based only on the gradient, especially when the actual phase jump between two adjacent pixels is larger than the modulation wavelength.

Another limitation is that phase jumps can only be detected based on the gradient surface of the neighboring measurements, which poses a problem, for example, when all measurements in the field-of-view are wrapped. For SAR systems, these limitations have been approached by including measurements from multiple modulation frequencies [9], [10]. In theory, a completely unwrapped signal can be reconstructed from two wrapped signals acquired with two mutually prime modulation frequencies. In practice, however, multi-frequency phase unwrapping is still challenging due to the measurement noise of ToF cameras.

In [11], we have applied phase unwrapping to ToF camera data captured at a single modulation frequency.

In this paper, we extend our previous work by adding information from multiple modulation frequencies to infer phase jumps in situations where a decision, only based on the gradient of neighboring measurements, is not possible. The remainder of this paper is organized as follows. The next section describes our probabilistic approach to phase unwrapping, including the use of multiple modulation frequencies. Sec. III presents results showing that the proposed method outperforms our previous approach which does not take multiple modulation frequencies into account.

II. PHASE UNWRAPPING

Throughout this chapter we are using an ongoing example to visualize the different steps of our approach to probabilistic phase unwrapping. We have chosen this particular example since the approach from our previous work [11] is not able to accurately determine the phase jumps in this scenario. A photo of the scene is shown in Fig. 2(a). The depth image in Fig. 2(b) is acquired using a SwissRanger SR4000 ToF camera from Mesa Imaging [13].

The camera is calibrated for a measurement range of 5 m. It supports different modulation frequencies, amongst others, 29 MHz, 30 MHz and 31 MHz with a non-ambiguity range of, respectively, 5.17 m, 5 m and 4.84 m. To obtain one corrected range image, we acquire two range images A and B at different modulation frequencies, with wavelengths $\lambda_A = 5.17$ m and $\lambda_B = 4.84$ m. In the following, B is only used to take multiple modulation frequencies into account, and A forms the basis for deriving the corrected range image. For our setup we deactivated the camera's internal averaging filters since they smooth the wrapped depth image.



Fig. 2. (a) An image of the scene. (b) Wrapped depth image from the ToF camera. A pixel's gray-scale value corresponds to the measured depth, from dark (close) to bright (far). The dark parts of the image indicate that distance measurements larger than 5 meters are wrapped.

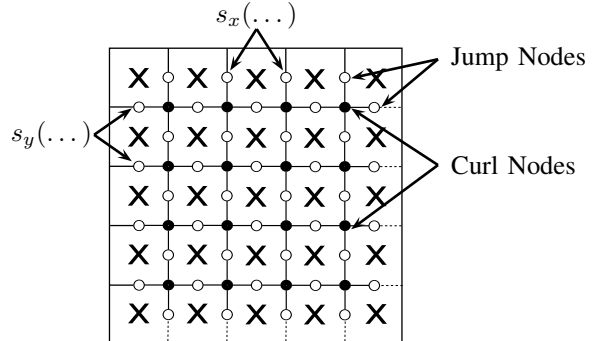


Fig. 3. The graphical model representing possible locations of phase jumps. The image pixels (black x's) are connected to their neighbors by jump nodes (white filled circles). Four jump nodes are connected by a curl node (black filled circles) which enforces the zero curl constraint.

To infer phase jumps between adjacent pixels, we use a graphical model which represents possible locations of relative phase jumps in x - and y -direction (see Fig. 3). The image pixels are connected to their neighbors by so-called *jump nodes*. These jump nodes represent the probability of a phase jump between two neighboring pixels. To assure consistency of phase jumps in a local neighborhood, we apply the idea of zero-curl constraints [12]. Four jump nodes are connected by a *curl node* that enforces local consistency of the individual jump configurations. Interaction between jump and curl nodes is achieved by passing messages across the graph that represent a node's belief. After convergence of the message passing, the detected phase jumps are integrated into the depth image by carrying out the respective projections, thereby correcting the erroneously wrapped distance measurements. The following subsections describe the above steps in detail.

A. Jump Nodes

Jump nodes represent the probability that a phase jump occurs between the two neighboring pixels. A phase jump in x -direction, i.e., between pixels (x, y) and $(x + 1, y)$, is denoted as $s_x(x, y)$. Jumps in y -direction, i.e., between pixels (x, y) and $(x, y + 1)$, are denoted as $s_y(x, y)$.

A phase jump can occur either in positive direction (-1), in negative direction (+1) or not at all (0). Considering the x -jumps, positive direction at pixel (x, y) means that there is

a phase jump between pixels (x, y) and $(x + 1, y)$. Negative means that the phase jump occurs between pixels $(x + 1, y)$ and (x, y) . The direction of a phase jump is important for the correction of distance measurements as it decides which and how the measurement needs to be corrected. The possible shift directions $(-1, 0, \text{and } 1)$ are called *jump configurations*.

Jump nodes are represented by a 3-element vector storing the probabilities for every jump configuration. The probabilities for a jump at a pixel location are calculated by the discontinuity term f_d fused with the frequency term f_f , which is described in the following.

1) *Discontinuity Term f_d* : The basic assumption behind the discontinuity term f_d is that neighboring measurements are more likely closer to each other than farther apart. This term increases the probability $P(s_{\{x,y\}}(x, y) = i | A, B)$, when the phase jump for configuration i brings the respective distance measurements closer together than the other configurations. Here we follow the formulation of [12]:

$$f_d(x, y, i) = \begin{cases} e^{-(\phi(x+1,y) - \phi(x,y) - i)^2 / 2\sigma^2}, & \text{for } s_x \\ e^{-(\phi(x,y+1) - \phi(x,y) - i)^2 / 2\sigma^2}, & \text{for } s_y \end{cases} \quad (1)$$

where $\phi(x, y)$ is the wrapped distance measurement for pixel (x, y) from the image A , scaled into the interval $[0, 1]$ (for simplicity, but without loss of generality) and σ^2 is the variance in the depth values between neighboring pixels in the wrapped image.

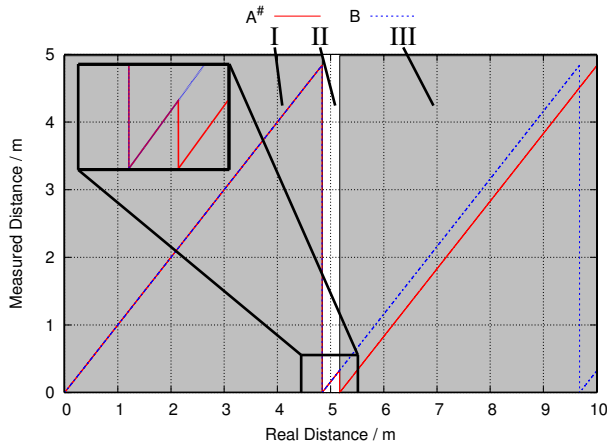


Fig. 4. The relationship between measurements $a^\#$ and b , acquired with two different modulation frequencies λ_A and λ_B .

2) *Frequency Term f_f* : To determine the frequency term f_f , depth images with two different modulation frequencies are acquired. The basic idea behind the frequency term is that, in the absence of noise, the range images acquired with the two modulation frequencies measure the same distance for those pixels that are not wrapped. In contrast, wrapped pixels show different distances due to the different non-ambiguity intervals. Ideally, these differences d should be equal to $(\lambda_A - \lambda_B)$ if measurements are wrapped in both depth images.

Note that measurements acquired with two different modulation frequencies have a non-overlapping part between λ_A

and λ_B . Therefore, we project the measurements $a \in A$ into the interval $(0, \lambda_B]$ obtaining a range image $A^\# = \{a \bmod \lambda_B | a \in A\}$.

As illustrated in Fig. 4, we obtain three regions by this projection. In regions I and II differences between distance measurements $a^\#$ and b are not measurable and $d(a^\#, b)$ is 0. In region III, where wrapped measurements occur, $d(a^\#, b)$ is close to $(\lambda_A - \lambda_B)$. In principal, under the assumption of ideal distance measurements, examining the differences $d(a^\#, b)$ allows for detecting all wrapped measurements and for constructing an unwrapped depth image.

We compute a reconstructed depth image \hat{R} only based on the frequency difference, where a pixel $\hat{r}(x, y)$ is defined as

$$\hat{r}(x, y) = \begin{cases} \phi(x, y) + 1, & \text{if } d(a^\#(x, y), b(x, y)) > \tau \\ \phi(x, y), & \text{else} \end{cases} \quad (2)$$

where the threshold τ is chosen based on $(\lambda_A - \lambda_B)$ and the camera's deviation in distance measurements. Those measurements that exceed the threshold are corrected by adding 1, i.e., unwrapping the distance measurement.

Since the measurements are subject to noise (especially when measuring poorly reflective objects), or caused by erroneous measurements (at jump edges, for example), a simple reconstruction based on \hat{R} is not possible. This can be seen in Fig. 5 showing the reconstructed depth image of the scene in Fig. 2. Wrapped pixels measured at plane surfaces with good reflection properties, e.g., the wall, are reconstructed correctly whereas pixels measured at the edges or on the ground are subject to reconstruction errors (indicated by the bright and dark spots). The reason for the reconstruction errors is that measurements at edges or poorly reflecting objects are subject to noise that exceeds $\pm(\lambda_A - \lambda_B)$. In our setup $(\lambda_A - \lambda_B)$ is 33 cm.

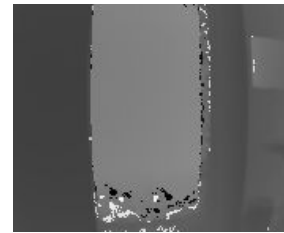


Fig. 5. The reconstructed depth image based on the difference of the two modulation frequencies.

For obtaining a frequency difference that is robust against noise, we do not consider individual pixels but take their local neighborhood into account. Referring to Fig. 6, for every jump node location we take medians $m_{\{x,y\}}^{\{\text{pos}, \text{neg}\}}$ in positive and negative direction each in x and y -direction over k adjacent pixels before and after an examined jump node. We determine m^{pos} and m^{neg} in, both, the wrapped range image A and the reconstruction \hat{R} that is solely obtained from $d(a^\#, b)$, as described above. For example, $m_{A,x}^{\text{pos}}$ is the horizontal median over the k adjacent pixels after an examined jump node in the wrapped depth image.

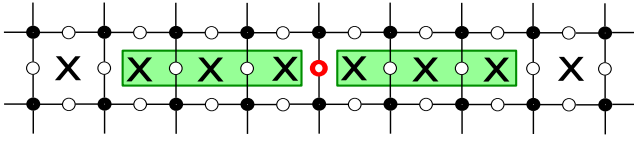


Fig. 6. For a given jump node (red/dark gray circle) the two neighborhoods (green/light gray boxes) are considered for taking the horizontal (x -direction) medians m_x^{pos} and m_x^{neg} .

In the following, we refer to these medians as $m_{A,\{x,y\}}^{\text{pos}}$, $m_{A,\{x,y\}}^{\text{neg}}$, $m_{\hat{R},\{x,y\}}^{\text{pos}}$, and $m_{\hat{R},\{x,y\}}^{\text{neg}}$. Analogous to Eq. 1, the frequency term is defined as

$$f_f(x, y, i) = \begin{cases} e^{-\frac{(|m_{\hat{R},x}^{\text{neg}} - m_{A,x}^{\text{neg}}| - |m_{\hat{R},x}^{\text{pos}} - m_{A,x}^{\text{pos}}| - i)^2}{2\sigma^2}}, & \text{for } s_x \\ e^{-\frac{(|m_{\hat{R},y}^{\text{neg}} - m_{A,y}^{\text{neg}}| - |m_{\hat{R},y}^{\text{pos}} - m_{A,y}^{\text{pos}}| - i)^2}{2\sigma^2}}, & \text{for } s_y. \end{cases}$$

If no phase jump between (x, y) and $(x + 1, y)$ occurred, $f_f(x, y, i)$ will be close to 1 for the configuration $i = 0$. More generally, depending on the actual configuration, $f_f(x, y, i)$ will be close to 1 for the respective configuration. Analogous to Eq. 1, the difference $|m_{\hat{R}}^{\text{neg}} - m_{A}^{\text{neg}}| - |m_{\hat{R}}^{\text{pos}} - m_{A}^{\text{pos}}|$ is approximately equal to the configuration i in case that a jump occurs at the examined node.

3) *Fusing f_d and f_f* : As can be seen in Fig. 7(a-d), solely using the discontinuity term f_d results in detections exactly localizing phase jumps while leaving a number of jumps undetected. In contrast, solely using the frequency term f_f accurately detects all phase jumps but causes a larger number of false positives. For fusing both terms we trust f_d with $c_d = 90\%$ and f_f with $c_f = 50\%$ (empirically determined), resulting in:

$$P(s_{\{x,y\}}(x, y) = i \mid A, B) \propto ((1 - c_d) + c_d f_d(x, y, i)) ((1 - c_f) + c_f f_f(x, y, i))$$

The result of combining and weighting f_d and f_f is shown in Fig. 7(e+f). It can be seen that the resulting detections are both accurate and exactly localized.

B. Curl Nodes

Four jump nodes are connected by a curl node which enforces the zero-curl constraint [12]. A curl node assures local consistency of the phase jumps, by summing up the shift configurations of the jump nodes around it. For example, the sum of the 4-pixel loop around (x, y) is $s_x(x, y) + s_y(x + 1, y) - s_x(x, y + 1) - s_y(x, y)$ (see Fig. 8). A zero-curl constraint is violated when a jump is not matched by another jump in the opposite direction, i.e., when the sum around a pixel loop is $\neq 0$. Therefore, the set of phase jumps for an image must satisfy the constraint

$$s_x(x, y) + s_y(x + 1, y) - s_x(x, y + 1) - s_y(x, y) = 0.$$

If all zero-curl constraints are satisfied, consistency of the inferred phase jumps in the complete image can be assumed.

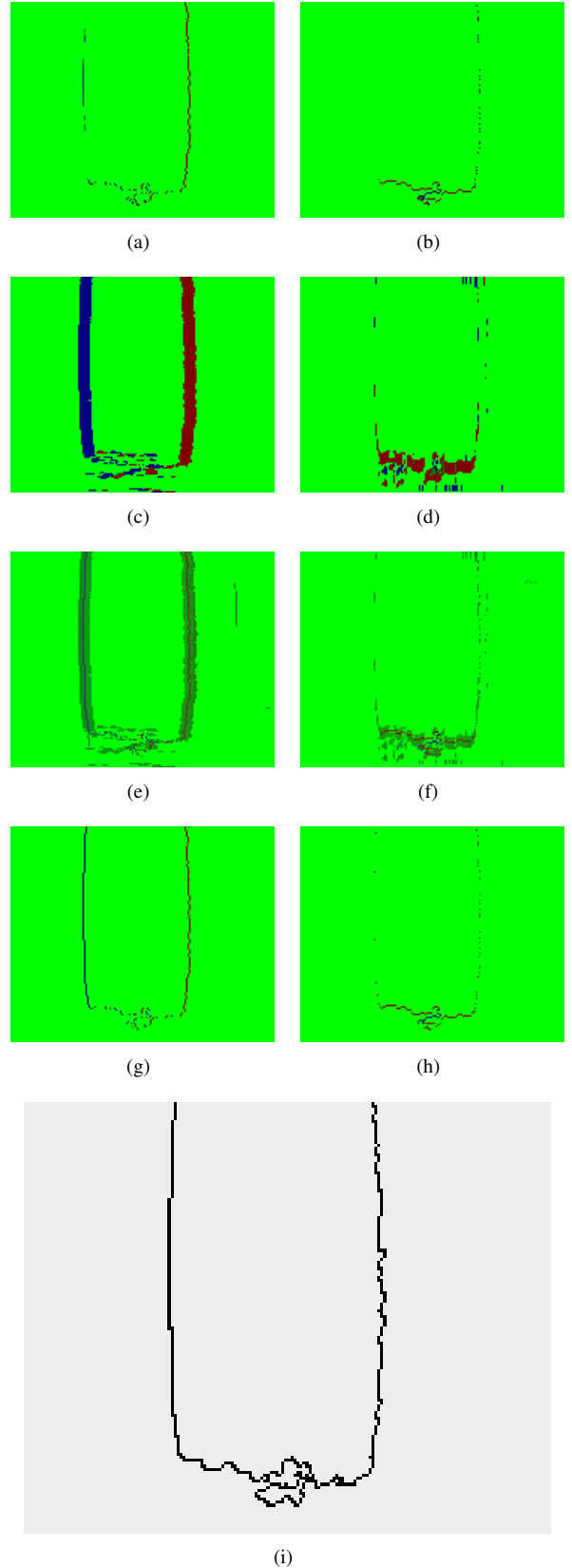


Fig. 7. The probabilities for the jump configurations $(-1, 0, 1)$ indicated by colors (blue, green, red). (a) + (b) The initial phase jump probabilities based on the depth discontinuity term f_d for the x and y -direction. (c) + (d) The initial phase jump probabilities based on the frequency term f_f . (e) + (f) The fusion of f_d and f_f . (g-i) The resulting phase jump configurations after belief propagation converged.

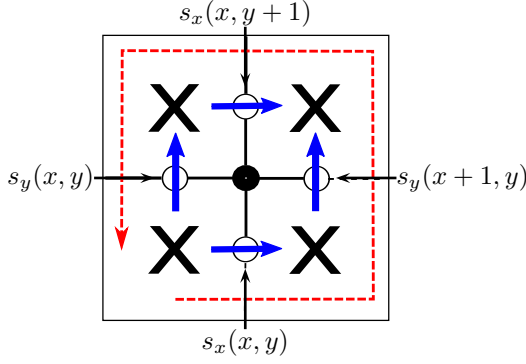


Fig. 8. A curl node assures local consistency of the phase shifts by summing up the shift configurations of the jump nodes around it (red dashed arrow), taking into account the direction of the jumps (blue arrows). A zero-curl constraint is violated when a jump is not matched by another jump in the opposite direction.

C. Message Passing

Inference of phase jumps is done by applying belief propagation (sum-product algorithm) in the graphical model. Messages, representing a node's belief of a configuration, are passed bi-directionally through the graph on the vertices between jump and curl nodes in a forward-backward-up-down type schedule.

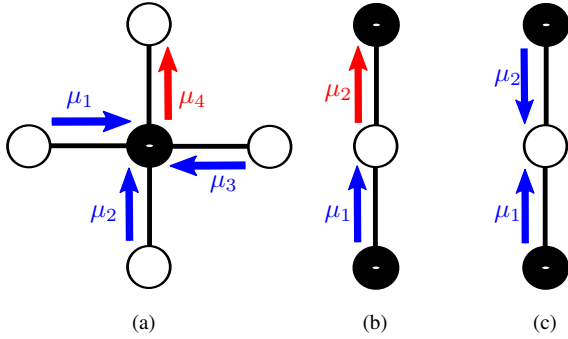


Fig. 9. (a) Messages from curl nodes to jump nodes (red arrows) are computed using incoming messages from jump nodes (blue arrows). (b) Messages from jump nodes to curl nodes are computed using incoming messages from curl nodes. (c) Messages from curl nodes to jump nodes are combined to approximate the marginal probability of a phase jump.

Messages are represented by 3-element vectors, where the elements are the probabilities for a specific configuration. As illustrated in Fig. 9(a), messages from curl nodes to jump nodes are calculated using incoming messages from jump nodes. For example, the outgoing message μ_{4i} depends on the incoming messages μ_1 , μ_2 and μ_3

$$\mu_{4i} = \sum_{j=-1}^1 \sum_{k=-1}^1 \sum_{l=-1}^1 \delta(k+l-i-j) \mu_{1j} \mu_{2k} \mu_{3l}$$

$$\text{with } \delta(x) = \begin{cases} 1, & x = 0 \\ 0, & \text{otherwise.} \end{cases}$$

Messages from the jump nodes to the curl nodes are

calculated using incoming messages from the curl nodes (Fig. 9(b)). For example, the outgoing message μ_2 is calculated from the incoming message μ_1 from the curl node by

$$\mu_{2i} = \mu_{1i} ((1 - c_d) + c_d f_d(x, y, i)) ((1 - c_f) + c_f f_f(x, y, i)).$$

The message vectors are normalized in every iteration. The marginal probabilities for the phase jumps are approximated by

$$\hat{P}(a(x, y) = i | A, B) = (\mu_{1i} \mu_{2i}) / \sum_{j=-1}^1 (\mu_{1j} \mu_{2j}).$$

When all zero-curl constraints are satisfied, the propagation of beliefs converges. The resulting jump configurations for the running example are shown in Fig. 7(g+h). Propagating the beliefs and combining the discontinuity term and the frequency term results in consistent and correct phase jump locations along x and y -directions. After convergence or when a fixed number of iterations is exceeded, the phase jumps are integrated into the wrapped depth image. Wrapped measurements can be localized by the position and the configuration of the x and y -direction phase jumps and corrected by adding the phase, i.e., λ_A . The phase jump locations for the example input image is shown in Fig. 7(h).

III. EXPERIMENTS

Two different experiments have been carried out in an indoor environment. In a first experiment, a scene with a continuous wall was chosen. The depth images from the scene can be unwrapped without employing the frequency term, since neighboring measurements are close together. Fig. 11 shows the wrapped and unwrapped depth images, as well as the resulting 3D point clouds. For this example, both the approach from our previous work and the proposed extension correctly unwrap the acquired depth image.

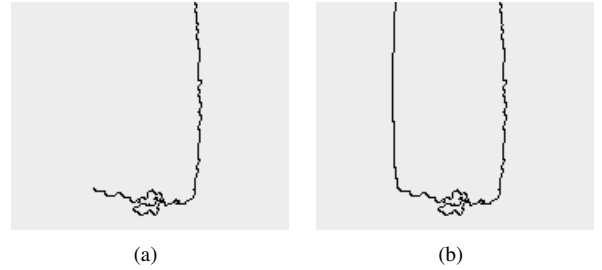


Fig. 10. (a) The resulting phase jumps without frequency term. (b) Phase jumps using the frequency term.

The second experiment in Fig. 12 shows a steep slope in neighboring depth measurements that contain discontinuities larger than $\lambda_A/2$. In this scenario, additional information based on the modulation frequencies is necessary. Without this additional information, i.e., making decisions solely based on distance discontinuities does not reliably unwrap the acquired depth image. Fig. 10(a) shows the resulting phase jumps without the frequency term. The resulting jumps

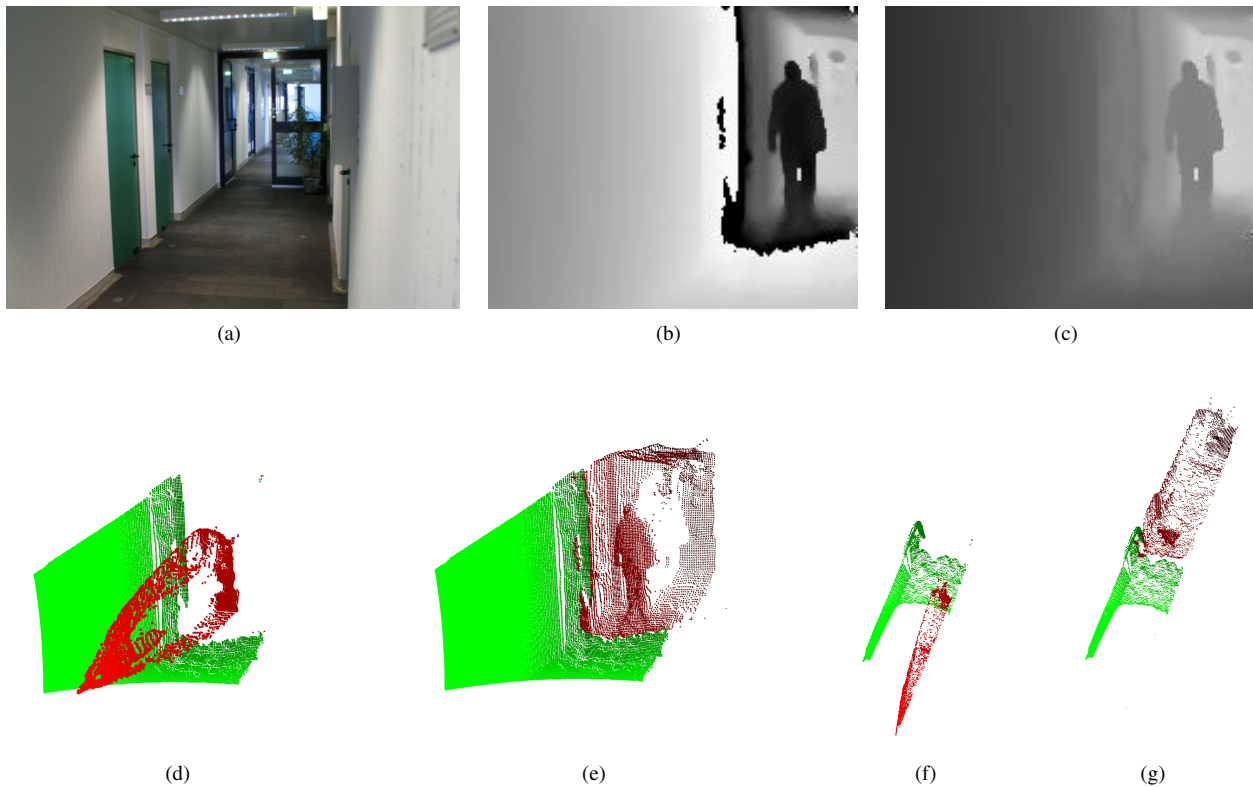


Fig. 11. (a) An image of the scene. (b) Wrapped depth image from the ToF camera. A pixel's gray-scale value corresponds to the measured depth, from dark (close) to bright (far). The dark parts of the image indicate that distance measurements larger than 5 meters are wrapped. (c) The unwrapped depth image. (d + f) The wrapped point clouds from two different perspectives. (e + g) The unwrapped point clouds. The color of the points indicate the result of the algorithm. Wrapped measurements are colored red.

are disconnected. Fig. 10(b) shows the resulting phase jumps obtained by including the introduced frequency term.

The experiments show that the depth images could be unwrapped successfully, even in scenes where phase unwrapping only based on depth discontinuity is not possible.

In the two experiments belief propagation converged in less than 5 iterations.

IV. CONCLUSIONS AND FUTURE WORK

We have presented a probabilistic approach for phase unwrapping specifically designed for handling ambiguities in ToF camera data. By means of a graphical model with loopy belief propagation, the approach does not only take into account discontinuities in the measured distances but also exploits multiple modulation frequencies to obtain accurate estimates of the locations where phase jumps have taken place.

The results show that the approach enables to correct ambiguous distance measurements such that the structure of the scene can be reconstructed correctly from wrapped depth images. This is an important result for the use of ToF cameras in the field of robotics, since current camera models, such as the SR4000 from Mesa, have a non-ambiguity range that is shorter than the maximum measurable distance of commonly used laser range scanners. Simply sorting out the wrapped measurements based on the ratio of distance and amplitude

does not work reliably in natural scenes, e.g., when highly reflective objects are sensed.

Especially in the context of 3D mapping, the ambiguity of the phase-shift based distance measurements prevented the use of ToF cameras for modeling larger environments where measured distances exceed the wavelength of the sensor's modulation frequency [4]. With correctly unwrapped depth images, we have, in principle, the ability of to model larger environments. However, it remains a matter of future work to actually apply probabilistic phase unwrapping for mapping a larger environment.

REFERENCES

- [1] J. W. Weingarten, G. Grüner, and R. Siegwart. A State-of-the-Art 3D Sensor for Robot Navigation. In *Proc. of the IEEE/RSJ International Conference on Intelligent Robots and Systems (IROS)*, pages 2155–2160, Sendai, Japan, 2004.
- [2] Raymond Sheh, M. Waleed Kadous, and Claude Sammut. On building 3d maps using a range camera: Applications to rescue robotics. Technical report, UNSW, Sydney, Australia, 2006.
- [3] K. Ohno, T. Nomura, and S. Tadokoro. Real-time robot trajectory estimation and 3d map construction using 3d camera. In *Proceedings of the IEEE/RSJ International Conference on Intelligent Robots and Systems (IROS)*, pages 5279–5285, 2006.
- [4] Stefan May, David Droschel, Dirk Holz, Stefan Fuchs, Ezio Malis, Andreas Nüchter, and Joachim Hertzberg. Three-dimensional mapping with time-of-flight cameras. *Journal of Field Robotics, Special Issue on Three-Dimensional Mapping, Part 2*, 26(11-12):934–965, December 2009.
- [5] Stefan Fuchs and Gerd Hirzinger. Extrinsic and Depth Calibration of ToF-Cameras. In *Proceedings of the IEEE International Conference on Computer Vision and Pattern Recognition (CVPR)*, 2008.

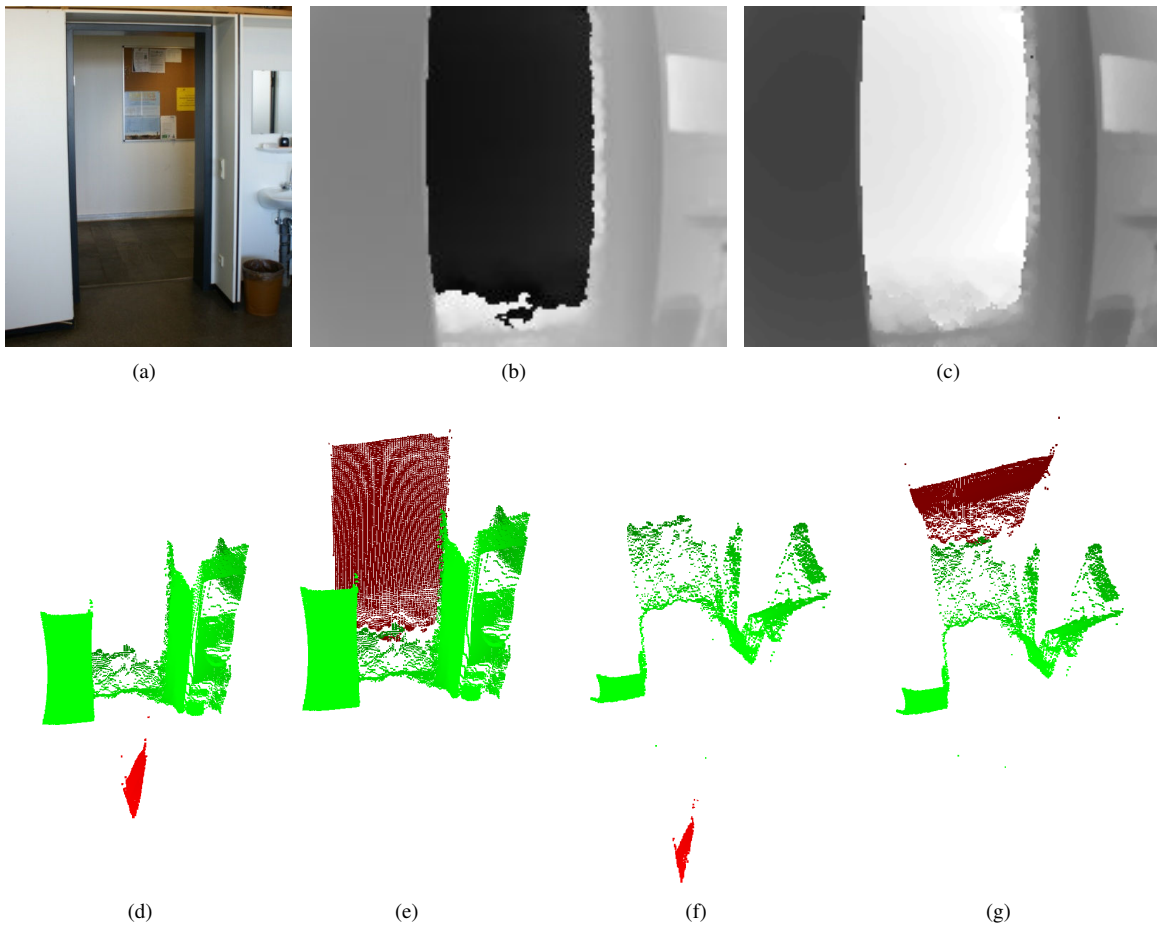


Fig. 12. (a) An image of the scene. (b) Wrapped depth image from the ToF camera. A pixel's gray-scale value corresponds to the measured depth, from dark (close) to bright (far). The dark parts of the image indicate that distance measurements larger than 5 meters are wrapped. (c) The unwrapped depth image. (d + f) The wrapped point clouds. (e + g) The unwrapped point clouds. The color of the points indicate the result of the algorithm. Wrapped measurements are colored red.

- [6] Dennis C. Ghiglia and Mark D. Pritt. *Two-Dimensional Phase Unwrapping: Theory, Algorithms, and Software*. Wiley-Interscience, 1998.
- [7] Z. Liang and P. Lauterbur. *Principles of Magnetic Resonance Imaging (A Signal Processing Perspective)*. IEEE Press, 1999.
- [8] Paul Thompson, Daniel E. Wahl, Paul H. Eichel, Dennis C. Ghiglia, and Charles V. Jakowatz. *Spotlight-Mode Synthetic Aperture Radar: A Signal Processing Approach*. Kluwer Academic Publishers, Norwell, MA, USA, 1996.
- [9] V. Pascazio and G. Schirinzi. Multifrequency insar height reconstruction through maximum likelihood estimation of local planes parameters. *Image Processing, IEEE Transactions on*, 11(12):1478–1489, dec 2002.
- [10] W. Xu, E.C. Chang, L.K.Kwoh, H.Lim, and A.Heng. Phase-unwrapping of sar interferogram with multi-frequency or multi-baseline. In *Proceed. Int. Geoscience and Remote Sensing Symposium*, pages 730–732, 1994.
- [11] David Droschel, Dirk Holz, and Sven Behnke. Probabilistic phase unwrapping for time-of-flight cameras. In *Proceedings of the joint conference of the 41st International Symposium on Robotics (ISR 2010) and the 6th German Conference on Robotics (ROBOTIK 2010), Munich, Germany*, pages 318–324, 2010.
- [12] Brendan J. Frey, Ralf Koetter, and Nemanja Petrovic. Very loopy belief propagation for unwrapping phase images. In Thomas G. Dietterich, Suzanna Becker, and Zoubin Ghahramani, editors, *NIPS*, pages 737–743. MIT Press, 2001.
- [13] Mesa Imaging AG. Swissranger tof cameras. <http://www.mesa-imaging.ch>.